

# JGR Space Physics

## RESEARCH ARTICLE

10.1029/2019JA027080

### Key Points:

- IpsDst giving the mean value of Dst during storm main phase represents the impulsive strength of geomagnetic storms
- IpsDst is better than other storm parameters (DstMin, Kpmax, AE<sub>max</sub>, IpsKp, and IpsAE) for space weather applications
- Geomagnetic storms of large IpsDst occur due to the impact of fast solar storms with IMF Bz southward at their front (or shock)

### Correspondence to:

N. Balan,  
balan.nanan@yahoo.com

### Citation:

Balan, N., Zhang, Q.-H., Shiokawa, K., Skoug, R., Xing, Z., Tulasi Ram, S., & Otsuka, Y. (2019). IpsDst of Dst storms applied to ionosphere-thermosphere storms and low latitude aurora. *Journal of Geophysical Research: Space Physics*, 124, 9552–9565. <https://doi.org/10.1029/2019JA027080>

Received 2 JUL 2019

Accepted 1 OCT 2019

Accepted article online 13 NOV 2019

Published online 21 NOV 2019

## IpsDst of Dst Storms Applied to Ionosphere-Thermosphere Storms and Low-Latitude Aurora

**N. Balan<sup>1,2</sup> , Qing-He Zhang<sup>1</sup>, K. Shiokawa<sup>3</sup>, R. Skoug<sup>4</sup>, Zanyang Xing<sup>1</sup>, S. Tulasi Ram<sup>5</sup>, and Y. Otsuka<sup>3</sup>**

<sup>1</sup>Institute of Space Sciences, Shandong University, Weihai, China, <sup>2</sup>Institute of Geology and Geophysics, Chinese Academy of Sciences, Beijing, China, <sup>3</sup>Institute for Space-Earth Environmental Research, Nagoya University, Nagoya, Japan, <sup>4</sup>Los Alamos National Laboratory, Los Alamos, NM, USA, <sup>5</sup>Indian Institute of Geomagnetism, Navi Mumbai, India

**Abstract** Conventionally, the minimum value of Dst (DstMin) and maximum values of Kp and AE (Kp<sub>max</sub> and AE<sub>max</sub>) representing the geomagnetic storm intensities have been used for investigating space weather in Earth's environment. The present paper uses the derived parameters (IpsDst, IpsKp, and IpsAE) giving the mean values of Dst, Kp, and AE during the main phase (MP) of Dst storms for investigating ionosphere-thermosphere storms and low-latitude (630 nm) aurora. The derived parameters (IpsDst, IpsKp, and IpsAE) representing the impulsive strength of geomagnetic storms seem to have more systematic dependence among themselves than among the intensities (DstMin, Kp<sub>max</sub>, and AE<sub>max</sub>). The ionosphere-thermosphere storms observed by the CHAMP (Challenging Minisatellite Payload) satellite and low-latitude auroras observed by optical imagers are much more intense during high impulsive storms than high intensity storms. In a statistical sense, over 175 positive ionospheric storms ( $\Delta$ NmF2) observed in 1985–2005 and the intensity of 20 red auroras observed in 1989–2004 at midlatitudes correlate better with the impulsive parameters than the intensity parameters, with the best correlation being with IpsDst. The mechanism of the impulsive action (high-energy input over a short duration) leading to large IpsDst arises from the impact of fast solar storms (interplanetary coronal mass ejections) with large IMF Bz southward at their front (or shock). The impulsive action results in bright low-latitude auroras and strong ionosphere-thermosphere storms.

## 1. Introduction

The paper for the first time applies the derived parameters IpsDst of Dst storms (Balan et al., 2016) and IpsKp and IpsAE of Kp and AE storms (section 2) for investigating ionosphere-thermosphere storms and low-latitude aurora, all caused by solar storms. The solar storms include interplanetary coronal mass ejections (ICMEs), high speed streams, and corotating interaction regions (e.g., Gopalswamy et al., 2005). They produce a series of rapid and sometimes severe changes in interplanetary space and the environment of planets (e.g., Witasse et al., 2017). The changes are collectively called space weather. An ICME is a huge, magnetized (interplanetary magnetic field IMF) (Interplanetary Magnetic Field) up to 100 nT, high density (up to 100 cm<sup>-3</sup>) plasma cloud ejected from the Sun and flowing out with speed up to thousands of kilometers per second (e.g., Skoug et al., 2004). However, the part of the ICME that is most geoeffective is the low density but high magnetic field region (Burlage et al., 1981). A high speed ICME produces shock waves ahead, which accelerate the background charged particles to high energies over 100 MeV, which are known as solar energetic particles or SEPs (Solar Energetic Particles) (e.g., Singh et al., 2010). The SEPs can damage satellite systems (e.g., Green et al., 2017) even more easily when they are accelerated further by the high speed ICME front that follows ICME shock (e.g., Balan et al., 2014).

The solar storms induce electric currents in Earth's magnetosphere producing disturbances in the geomagnetic field. The disturbances lasting from several hours to several days are the geomagnetic storms (Gonzalez et al., 1994; Kamide et al., 1998; Lühr et al., 2017; Svalgaard, 1977). The current systems in the magnetosphere contribute differently to the storms in different latitudes, and the storms are therefore identified by the indices such as the low-latitude Dst (disturbance storm time) index (Love & Gannon, 2009; Sugiura, 1964), midlatitude Kp index, and high-latitude AE index (e.g., Rostoker et al., 1995). Another index sometimes used is the rate of change of the horizontal component (dH/dt) of the geomagnetic field. The Dst storms arise mainly from the intensification of the ring current due to ICME-magnetosphere coupling and

ionosphere-ring current coupling, the efficiency of which has been studied using solar wind and IMF data and models (e.g., Burton et al., 1975; Fok et al., 2001; Ebihara et al., 2005; Newell et al., 2007; Liemohn et al., 2010). The storms become stronger and more intense with the increase in the solar wind velocity and strength of IMF Bz southward.

The increases and decreases in the density, temperature, electric fields, and currents happening in the ionosphere during geomagnetic storms are the positive and negative ionospheric storms (e.g., Balan & Rao, 1990; Rishbeth, 1991; Batista et al., 1991; Fuller-Rowell et al., 1994; Prolss, 1995; Tulasi Ram et al., 2012, 2015). In density, usually positive storms occur first especially during daytime and negative storms follow at low and midlatitudes except around the equator (e.g., Balan et al., 2013; Lu et al., 2012; Mendillo, 2006; Sojka et al., 2012). The density in extreme cases increases over 1,000% of the quiet time levels, especially around the daytime equatorial ionization anomaly (EIA) crests, which shift from their normal locations of  $\sim\pm 15^\circ$  to  $\pm 30^\circ$  magnetic latitudes (e.g., Balan et al., 2011; Mannucci et al., 2005). The density during negative ionospheric storms decreases down to very low levels compared to quiet time values (e.g., Vijaya Lekshmi et al., 2011). The changes in thermospheric density, composition, and wind velocity are the thermospheric storms (e.g., Liu & Luhr, 2005; Mayr & Volland, 1973; Roble et al., 1982).

The auroras become bright, extend to lower than normal latitudes, and can sometimes be observed from low latitudes during geomagnetic storms (e.g., Hayakawa et al., 2018; Kataoka et al., 2017; Loomis, 1861; Shiokawa et al., 1999). The low-latitude auroras are typically characterized by (1) the  $N_2^+ + N$  emission at high vibrational levels and (2) a high ( $>10$ ) ratio of red (630.0 nm) to green (557.7 nm) atomic oxygen lines (Tinsley et al., 1984). The latter aurora sometimes shows intense visible emissions, producing a spectacular red aurora in the sky (Shiokawa et al., 2013). Recent studies report that the red auroras appear during the main phase (MP) of geomagnetic storms and last from a few hours to several hours (Rassoul et al., 1992). Recently, Shiokawa et al. (2005) reported a list of 20 low-latitude auroras observed in Japan.

For investigating the different aspects of the Earth's surrounding space weather (examples above), it has been important to identify some parameters of the geomagnetic storms. Conventionally, DstMin (maximum negative value of Dst during storm main phase MP),  $(dDst/dt)_{MPmax}$  (maximum rate of change of Dst during MP),  $(dH/dt)_{max}$ , and maximum values of Kp and AE ( $Kp_{max}$  and  $AE_{max}$ ), all representing geomagnetic storm intensity, have been used for this purpose. However, while studying what determines the severity of the space weather, we realized that the storm intensity (DstMin) is insufficient to distinguish between the severe space weather (SvSW) causing electric power outages and telegraph system failures and normal space weather not causing such severe effects (Balan et al., 2014). Our studies also showed that the mean value of Dst during MP ( $\langle Dst_{MP} \rangle$ ) can indicate the severity of space weather (Balan et al., 2016). It can also be used as a better reference than DstMin in developing a scheme for forecasting SvSW using ICME velocity  $V$  and IMF Bz (Balan, Ebihara, et al., 2017). Hereafter, we refer the parameter  $\langle Dst_{MP} \rangle$  as IpsDst (section 2).

The present paper applies the parameter IpsDst derived for the storms ( $DstMin \leq -50$  nT) automatically identified in Kyoto Dst (Balan, TulasiRam, et al., 2017) to investigate ionospheric storms, thermospheric storms, and low-latitude aurora. In addition to IpsDst, the paper uses DstMin,  $Kp_{max}$ ,  $AE_{max}$ ,  $\langle Kp_{MP} \rangle$  (or IpsKp), and  $\langle AE_{MP} \rangle$  (or IpsAE) for comparisons. For ionosphere-thermosphere storms, the paper uses the ionospheric electron density (Ne) and thermospheric mass density ( $\rho$ ) measured by the CHAMP satellite (Reigber et al., 2002) and ionospheric peak electron density (NmF2) measured by an ionosonde in Japan for 20 years (1986–2005). For low-latitude aurora, the paper uses the auroral intensity measured by optical instruments in Japan during 20 low-latitude auroras in 1998–2004 (Shiokawa et al., 2005). For discussing the physical mechanism connecting the geophysical storms to the corresponding solar storms, the paper uses the solar wind and IMF data from the ACE (Advanced Composition Explorer) satellite available since 1998 (McComas et al., 1998). Section 2 describes the data and analysis. The results are presented and discussed in sections 3 and 4. It will be shown that IpsDst is a better parameter than other parameters for investigating a variety of space weather aspects.

## 2. Data and Analysis

The hourly Dst data since 1957 are available at the Kyoto world data center (WDC) at <http://wdc.kugi.kyoto-u.ac.jp/dstdir/>. The Kp and AE data are available at Kyoto WDC at <http://wdc.kugi.kyoto-u.ac.jp/kp/index>.

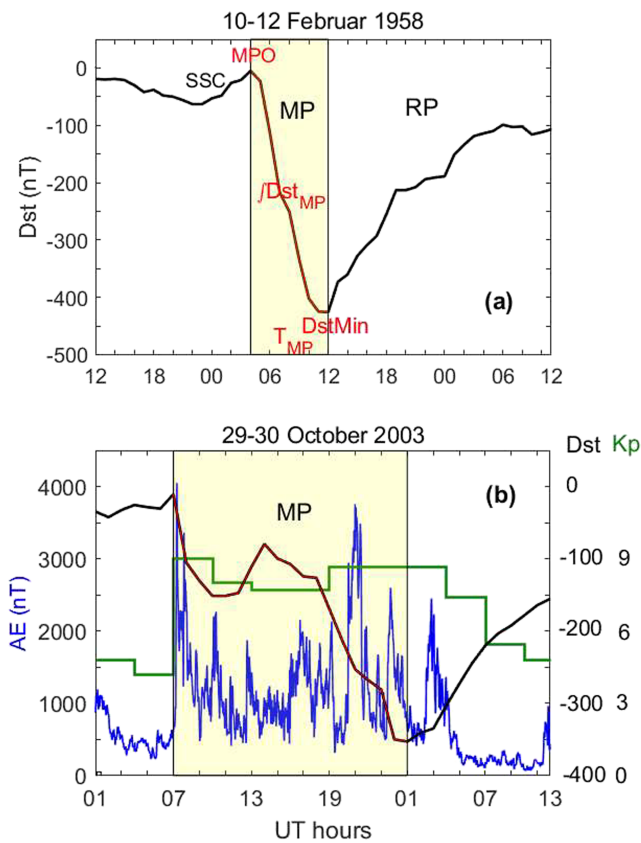


**Figure 1.** Examples (a) showing Dst storm characteristics and (b) identifying the storm main phase MP in Dst, K<sub>p</sub>, and AE storms.

Wind Ion) mode of the SWEPAM (Solar Wind Electron Proton Alpha Monitor) instrument at 64-s resolution (e.g., McComas et al., 1998; Skoug et al., 2004) are available at Caltech (<http://www.srl.caltech.edu/ACE/ASC/>). During high-energy particle events, when the SWI mode may not cover the full solar wind flux distribution, the 64-s data collected in the search/supra thermal ion mode once every  $\sim$ 32 min will be used. The velocity  $V$  and IMF  $B_z$  data corresponding to several super Dst storms will be used in the discussions. The data (time) are shifted for the ACE-Earth distance.

## 2.1. Derived Parameters

The parameter IpsDst is defined as (Balan et al., 2016)

$$\text{IpsDst} = (-1/T_{\text{MP}}) \int_{\text{MPO}}^{\text{RP}} |\text{Dst}_{\text{MP}}| dt$$

As shown in Figures 1a,  $T_{\text{MP}} |\text{Dst}_{\text{MP}}| dt$  is the integral (or sum) of the modulus of Dst from MPO to Dst<sub>Min</sub>. MPO is the MP onset time when Dst starts decreasing satisfying the storm selection criteria (and IMF  $B_z$  turning southward), which is also the peak of the storm sudden commencement (SSC).  $T_{\text{MP}}$  is the time interval (or duration) of the storm MP from MPO to Dst<sub>Min</sub>. The program also calculates the values of  $(d\text{Dst}/dt)_{\text{MPmax}}$ . By definition, the parameter IpsDst includes most important characteristics of Dst storms (SSC, MPO,  $(d\text{Dst}/dt)_{\text{MPmax}}$ , Dst<sub>Min</sub>, and  $T_{\text{MP}}$ ) and gives the mean value of Dst during the MP when most energy input occurs (Figure 1a). IpsDst is proportional to the total amount of energy input during MP (e.g., Burton et al., 1975) divided by the duration of energy input. The higher the energy input and shorter the duration, the larger its value and more impulsive its action. It therefore indicates the *impulsive (Ips)* strength of Dst storms and so is called IpsDst. Slow and fast varying MPs typically do not give equal values of IpsDst because the MPs in most cases fluctuate and their slopes change with time.

html and <http://wdc.kugi.kyoto-u.ac.jp/aedir/>, respectively. The Dst storms are automatically identified by a computer program that uses four selection criteria. The criteria are (1)  $\text{Dst}_{\text{Min}} \leq -50$  nT and  $T_{\text{MP}} > 2$  hr, (2) absolute value of MP range, that is,  $|\text{Dst}_{\text{MPO}} - \text{Dst}_{\text{Min}}| \geq 50$  nT, (3) separation between  $\text{Dst}_{\text{Min}}$  and next MPO  $\geq 10$  hr, and (4) rate of change of Dst during MP or  $(d\text{Dst}/dt)_{\text{MP}} < -5$  nT/hr. MPO here stands for MP onset and  $T_{\text{MP}}$  represents the MP time duration. The selection criteria minimize nonstorm like fluctuations and identified 793 storms in 1957–2007 (Balan, TulasiRam, et al., 2017). The storms include 39 super storms ( $\text{Dst}_{\text{Min}} \leq -250$  nT), 308 intense storms ( $-250 < \text{Dst}_{\text{Min}} \leq -100$  nT), and 446 moderate storms ( $-100 < \text{Dst}_{\text{Min}} \leq -50$  nT).

The ionospheric electron number density ( $N_e$ ) and thermospheric mass density ( $\rho$ ) measured by the CHAMP satellite (Reigber et al., 2002) at  $\sim$ 400-km altitude during several super Dst storms will be used for investigating the storm time variations of  $N_e$  and  $\rho$  with IpsDst and other parameters. The statistical correlations of ionospheric storms with IpsDst and other parameters will be obtained using the ionospheric peak electron density (NmF2) measured at the midlatitude station Kokubunji (35.7°N, 139.5°E; 26.8°N magnetic latitude) in Japan in 1985–2005 (<http://wdc.nict.go.jp/IONO/HP2009/ISDJ/index-E.html>). The red auroras observed at Rikubetsu (43.5°N, 143.8°E; magnetic latitude 34.7°N) and Moshiri (44.4°N, 142.3°E; magnetic latitude 35.5°N) in Japan (Shiokawa et al., 2005) will be used for investigating the intensity of the low-latitude auroras with IpsDst and other parameters. Though the auroral observations were made at midlatitudes, we use the phrase “low-latitude aurora” implying that they occur at much lower latitudes than normal auroras and to be consistent with earlier studies (e.g., Shiokawa et al., 2005, 2013).

The ACE satellite at the L1 point provides continuous solar wind and IMF data since 1998. The velocity and density data in the SWI (Solar

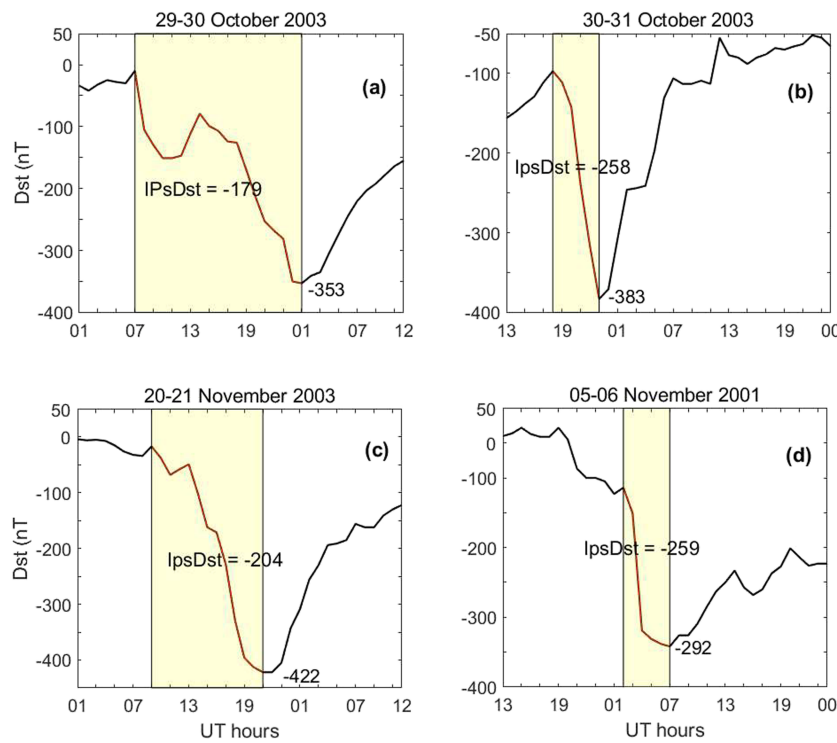


**Figure 2.** Four super Dst storms, two with larger IpsDst (30 October 2003 and 6 November 2001) and other two with comparatively smaller IpsDst (29 October 2003 and 20 November 2003).

The maximum values of the Kp and AE storms ( $K_{\text{p}}^{\max}$  and  $AE_{\max}$ ) are noted. The MP durations of the Kp and AE storms corresponding to the MP of a Dst storm are identified as shown in Figure 1b. The mean values of Kp and AE during the storm MP are calculated as

$$\langle K_{\text{p}}^{\text{MP}} \rangle = \sum K_{\text{p}}^{\text{MP}} / T_{\text{MP}} \quad \text{and} \quad \langle AE_{\text{MP}} \rangle = \sum AE_{\text{MP}} / T_{\text{MP}}.$$

For consistency, we use IpsKp and IpsAE to denote  $\langle K_{\text{p}}^{\text{MP}} \rangle$  and  $\langle AE_{\text{MP}} \rangle$ , respectively. IpsKp and IpsAE seem to represent the impulsive strengths of Kp and AE storms because they give the mean values of Kp and AE during the storm MP when most energy input occurs. The accuracy of IpsDst (and IpsKp and IpsAE) depends on the accurate identification of the times of MPO and DstMin. The computer program identifies these times following the selection criteria. The MPO times of the intense and super storms since 1998, when ACE data are available, are checked and found agreeing with the times of IMF Bz turning southward. According to the scientists (Sugiura & Kamei, 1991) who derived the Dst index, its uncertainty is mainly due to the errors in the magnetometer measurements at the four Dst observatories and Sq error, which are not easy to compute (T. Iyemori, private communication, 22 June 2019). However, these errors affect both IpsDst and DstMin almost equally. IpsDst therefore may probably be as accurate as DstMin.

### 3. Results

#### 3.1. Typical Geomagnetic Storms

Figure 2 shows four super Dst storms, two with large IpsDst (30 October 2003 and 6 November 2001) and other two with comparatively weak IpsDst (29 October 2003 and 20 November 2003). The top of the figures notes the storm days. The parameters of the Dst storms and of the corresponding Kp and AE storms are listed in Table 1, though the Kp and AE storms are not shown for simplicity. As listed, the super storms (1 and 2) on 30 October 2003 and 6 November 2001 that have large IpsDst (-258 and -259 nT) also have large IpsKp (9 and 8+) and IpsAE (1,816 and 1,675 nT). These storms have short MPs with almost no fluctuations (Figure 2). The other two super storms (3 and 4) on 29 October 2003 and 20 November 2003, which have

**Table 1***Number, Date, and Parameters of Geomagnetic Storms, Ionosphere-Thermosphere Storms, And Low-Latitude Aurora*

No.	Date	DstMin (-nT)	IpsDst (-nT)	Kp <sub>max</sub>	IpsKp	AE <sub>max</sub> (nT)	IpsAE (nT)	ΔNe <sub>max</sub> ( $\times 10^5$ cm <sup>-3</sup> )	Δρ <sub>max</sub> ( $\times 10^5$ cm <sup>-3</sup> )	Au_Int (kR)
1	30 Oct 2003	383	258	9	9	3,282	1,816	69.0	20.3	3.5
2	6 Nov 2001	292	259	9-	8+	3,296	1,675	42.7	Nan	4.0
3	29 Oct 2003	353	179	9	8+	4,056	1,307	15.4	12.1	2.2
4	20 Nov 2003	422	204	9-	8	4,192	1,247	11.9	5.5	1.4

Note. The parameters of four super geomagnetic storms (DstMin, IpsDst, Kp<sub>max</sub>, IpsKp, AE<sub>max</sub>, and IpsAE), strength of corresponding ionosphere-thermosphere storms (ΔNe<sub>max</sub> and Δρ<sub>max</sub>), and intensity of low-latitude aurora (Au\_Int).

comparatively smaller IpsDst (-179 and -204 nT) also have smaller IpsKp (8+ and 8) and IpsAE (1,307 and 1,247 nT). They have long MPs with fluctuations. However, the storm intensities (DstMin, Kp<sub>max</sub>, and AE<sub>max</sub>) do not have such systematic dependence. For example, the most intense super storm of solar cycle 23 (20 November 2003) has the largest DstMin (-422 nT) and AE<sub>max</sub> (4,192 nT) but comparatively weak IpsDst (-204 nT) and IpsKp (8). In short, the impulsive strength (IpsDst, IpsKp, and IpsAE) of the storms seems to have more systematic dependence among themselves than among the storm intensities (DstMin, Kp<sub>max</sub>, and AE<sub>max</sub>). The following sections will present the ionosphere-thermosphere storms and low-latitude auroras during the super storms (Figure 2).

### 3.2. Ionosphere-Thermosphere Storms

Figures 3 and 4 show the peak ionosphere-thermosphere responses during the super storms shown in Figure 2. The thick curves (number 1) display the latitude variations of the electron density (Ne) and neutral mass density ( $\rho$ ) at ~400-km altitude measured by the CHAMP satellite at the peak of the ionosphere-thermosphere storms, and thin curves (number 2) show the corresponding previous quiet day variations. For each storm, the latitude variations of Ne and  $\rho$  during all satellite passes from MPO to the end of RP (recovery phase) are compared with the corresponding previous quiet time data. The satellite pass that gave the maximum difference (ΔNe<sub>max</sub> and Δρ<sub>max</sub>) between the storm time data and quiet time data is considered to correspond to the peak of the ionosphere-thermosphere response (Balan et al., 2011). All panels use the same Y axes scale for comparison.

Out of the 10 super storms observed by CHAMP, the only two storms (30 October 2003 and 6 November 2001) having large IpsDst (-258 and -259 nT) show very strong ionospheric storms, with the one on 30 October 2003 (Figure 3b) being the strongest (see also Balan et al., 2011; Mannucci et al., 2005). The ionospheric storm on 6 November 2001 (Figure 3d) also would have been very strong (as on 30 October 2003), if the local time of the satellite pass were around noon instead of evening (MLT ~19). The Dst storms on 29 October 2003 and 20 November 2003 having comparatively weak IpsDst (-179 and -204 nT) are associated with weak ionospheric storms (Figures 3a and 3c). Table 1 lists the strength of the ionospheric storms (ΔNe<sub>max</sub>). As listed, the ΔNe<sub>max</sub> values during the high impulsive Dst storms (1 and 2) are over four times greater than those during the low impulsive storms (3 and 4), though the low impulsive storm on 20 November 2003 is the most intense according to DstMin (-422 nT). Though the storms (Figure 3) correspond to the same season at high solar activity, the local time difference of the MP can cause some differences in the ionospheric storms.

The variations of  $\rho$  measured by CHAMP during the same orbits as Ne are displayed in Figure 4. However, for 30 October 2003, the variation of  $\rho$  during the previous orbit (90 minutes before the peak of the ionospheric storm) is shown to illustrate the huge neutral surge from high latitudes flowing fast toward the equator. No neutral density data are available for 6 November 2001. Comparing the three cases in Figure 4, the fast equatorward neutral surge followed by fast wind, predicted by theoretical models (Fuller-Rowell et al., 1994), is observed only during the high impulsive storm on 30 October 2003 having large IpsDst = -258 nT (Figure 4b). For the other two cases having comparatively weak IpsDst, there was no equatorward neutral surge but only (slow) equatorward winds (Figures 4a and 4c). As listed in Table 1, the thermospheric storm (Δρ<sub>max</sub>) during the high impulsive storm is up to about 4 times as strong as those during low impulsive storms.

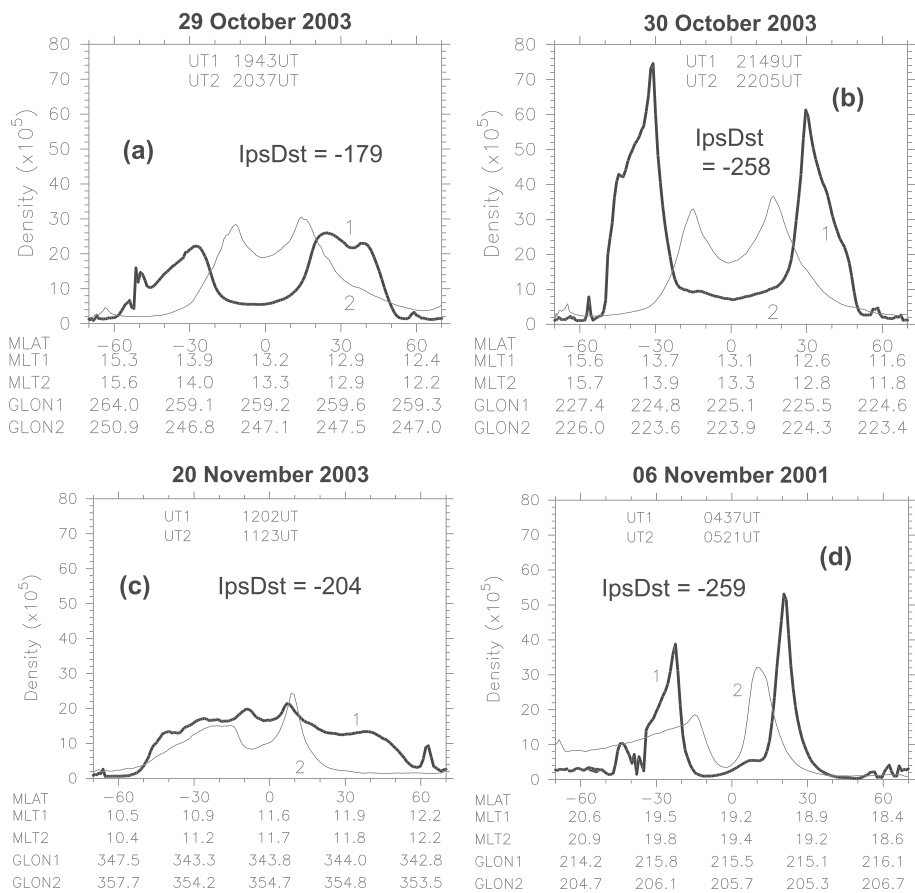


**Figure 3.** Latitude variations of electron density  $Ne$  at  $\sim 400$ -km altitude measured by CHAMP satellite at the peak of the ionospheric storms (thick curves 1) during the four super storms shown in Figure 2, together with previous quiet time variations (thin curves 2). Storm days are noted at the top. Equatorial crossing times of the satellite are noted inside each figure, and magnetic latitudes, longitudes, and local times of the satellite passes are listed at the bottom. All panels use the same Y axes scale for comparison.

Figure 5 shows the statistics of positive ionospheric storms. It shows scatter plots of the maximum positive deviation of the peak electron density ( $\Delta NmF2$ ) against  $IpsDst$  and  $DstMin$ . As mentioned in section 2, the  $NmF2$  data were measured at the midlatitude station Kokubunji in 1985–2005. During this period, 303 Dst storms ( $DstMin \leq -50$  nT) were identified, of which 191 are associated with positive ionospheric storms. For each geomagnetic storm, the maximum positive (and negative) difference ( $\Delta NmF2$ ) between the storm day  $NmF2$  and five previous quiet day average  $NmF2$  gives the maximum positive (and negative) ionospheric storm. As shown,  $\Delta NmF2$  is better correlated with  $IpsDst$  ( $\sigma = 0.61$ ) than  $DstMin$  ( $\sigma = 0.52$ ). The scatter of  $\Delta NmF2$  indicates the diurnal, seasonal and solar activity dependencies of ionospheric storms. Earlier, using manual Dst storm selection, Vijaya Lekshmi et al. (2011) identified 584 storms ( $DstMin \leq -50$  nT) in the same period (1985–2005) of which 255 were associated with positive storms in  $NmF2$  at Kokubunji, and  $\Delta NmF2$  showed a correlation of 0.34 with  $DstMin$ . Compared to  $IpsDst$  (and  $DstMin$ ),  $\Delta NmF2$  is found to have smaller correlations with other parameters ( $Kp_{max}$ ,  $AE_{max}$ ,  $IpsKp$ , and  $IpsAE$ ), not shown for simplicity.

However, the correlation of the negative ionospheric storms ( $-\Delta NmF2$ ) with  $IpsDst$  ( $\sigma = 0.49$ ) is found not improved compared to that with  $DstMin$  ( $\sigma = 0.53$ ), not shown. This may be because it is only the positive storms that are directly driven by the external forces. The larger the  $IpsDst$  (representing the impulsive strength of the external forces) the stronger the positive storms. The negative storms (at midlatitudes) are due to the internal thermospheric composition change (or  $O/N_2$  decrease) which becomes effective after or toward the end of the majority of the main energy input, discussed in section 4.

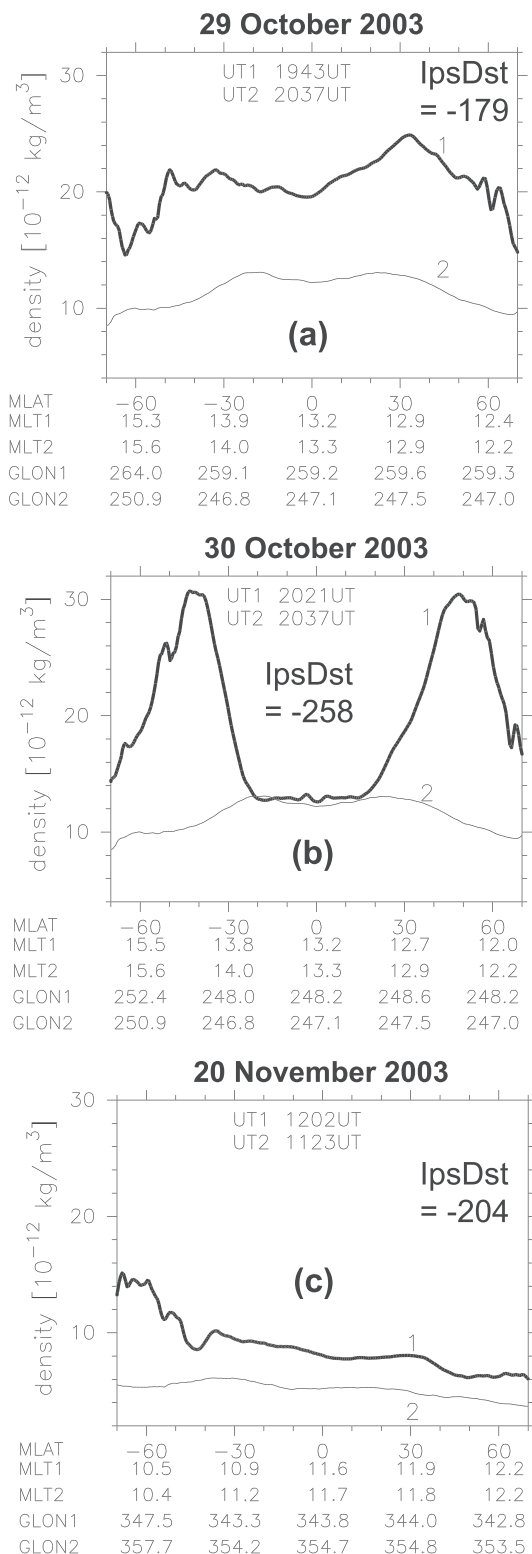


**Figure 4.** Latitude variations of the neutral mass density ( $\rho$ ) measured by CHAMP during the same orbits as in Figure 3. However, for 30 October 2003, the variation of  $\rho$  during the previous orbit is shown, and no  $\rho$  data for 6 November 2001, see text.

### 3.3. Low-Latitude Aurora

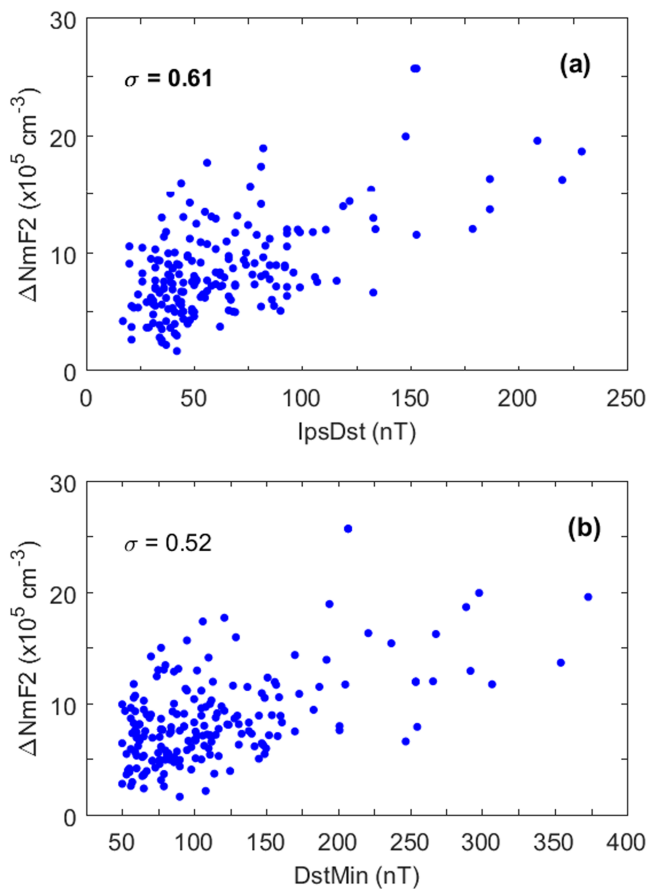
Here we use IpsDst and other parameters for investigating low-latitude aurora. As mentioned in section 1, auroras at middle and low latitudes have been observed visually during intense geomagnetic storms for many centuries in different parts of the world (e.g., Hayakawa et al., 2018; Loomis, 1861). Shiokawa et al. (2005) listed 20 low-latitude auroral events recorded at Rikubetsu (magnetic latitude  $34.7^\circ\text{N}$ ) and Moshiri (magnetic latitude  $35.5^\circ\text{N}$ ) in Japan in 1989–2004. The auroras appeared during geomagnetic storms at high solar activity and lasted from a few hours to the whole night in some cases. The intensities of the 630.0-, 557.7-, and 427.8-nm wavelengths were observed using highly sensitive optical instruments (all-sky cooled-CCD (Charged-Coupled Device) imagers and tilting photometers) (Shiokawa et al., 1999). We use the intensities of the red auroras at a wavelength of 630.0 nm.

Figure 6 shows examples at the peak of three red auroras observed at Rikubetsu during the Dst storms on 20 November 2003 ( $\text{DstMin} = -422 \text{ nT}$ ,  $\text{IpsDst} = -204 \text{ nT}$ ), 29 October 2003 ( $\text{DstMin} = -353 \text{ nT}$ ,  $\text{IpsDst} = -179 \text{ nT}$ ), and 30 October 2003 ( $\text{DstMin} = -383 \text{ nT}$ ,  $\text{IpsDst} = -258 \text{ nT}$ ). The top of the images is to the north and left is to the east; the color scale is the same for all cases. Of the three cases, the aurora was most intense, covered a wide field of view, and lasted the whole night on 30 October 2003, which corresponds to the high impulsive storm with large IpsDst ( $-258 \text{ nT}$ ). Of all images recorded at Rikubetsu since 1998, the poleward edge of the low-latitude aurora was observed only for this (30 October 2003) event.

Figure 7 shows scatterplots of the peak intensity of the auroras against geomagnetic storm parameters. Blue and red dots correspond to Moshiri and Rikubetsu data, respectively. Since the auroras originate at high latitudes, in addition to the correlations with IpsDst and  $\text{DstMin}$ , the correlations with  $K_p$  and  $\text{IpsKp}$ , and  $\text{AE}_{\max}$  and  $\text{IpsAE}$  are shown. It is interesting to note that the auroral intensity is correlated better with the impulsive strengths of geomagnetic storms (Figures 7d–7f) than their intensities (Figures 7a–7c); highest correlation is with the impulsive strength IpsDst of Dst storms ( $\sigma = 0.73$ ); and lowest correlation is with the high latitude storm parameters ( $\text{AE}_{\max}$  and  $\text{IpsAE}$ ). As listed in Table 1, the peak intensity during the high impulsive storms (30 October 2003 and 6 November 2001) is nearly double that during the low impulsive storms (29 October 2003 and 20 November 2003).

## 4. Discussion

As mentioned in section 1, Dst storms have been studied and modeled for many years using solar wind and IMF data. For example, using  $V$ ,  $N$  (density), and  $Bz$ , Burton et al. (1975) modeled the seven Dst storms in 1967–1968. Klimas et al. (1997) presented a method for transforming a linear prediction model into linear and nonlinear dynamical analogs of the coupling between the input and output data. Using  $VBz$  for input and  $Dst$  for output, they showed that the nonlinear analog couples to the solar wind through the expression  $(VBz/Dst) \times VBz$  rather than through the usual linear dependence on  $VBz$ . The multi-input ( $VBz$  and dynamic pressure  $P$ ) and single-output ( $Dst$ ) discrete time model developed by Zhu et al. (2007) explains the  $Dst$  dynamics more accurately than previous models. Using USGS (United States Geological Survey)  $Dst$  and a lognormal



**Figure 5.** Statistics of ionospheric storms ( $\Delta NmF2$ ) at Kokubunji in Japan in 1985–2005 and correlations with  $IpsDst$  and  $DstMin$ .

The positive storms at midlatitudes turn to negative storms when the composition change effect of ENW (decrease of  $O/N_2$ ) takes over its mechanical effects. The MPs occurring at night, when there is no production of ionization, generally lead to negative ionospheric storms at midlatitudes. However, in some cases, nighttime MPs lead to comparatively weak positive ionospheric storms during the following daytime. This may be because the night MPs extends to the following daytime or the nighttime MPs may be of large  $IpsDst$ . At around the equator, negative ionospheric storms occur during daytime MPs due to super plasma

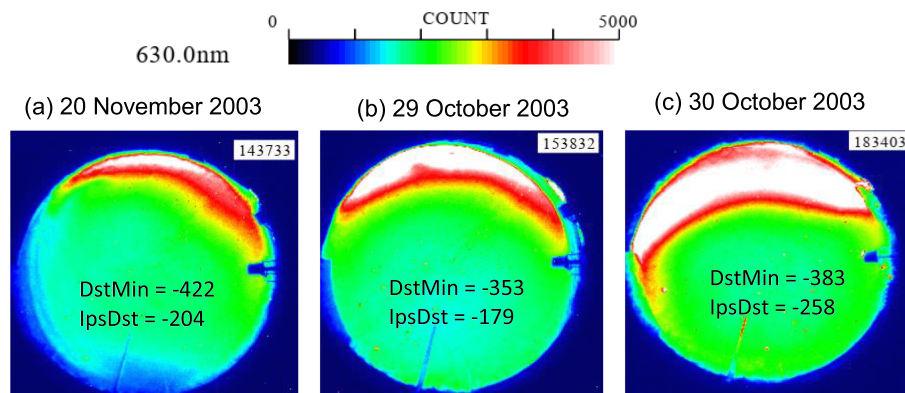


**Figure 6.** Examples of aurora during the high impulsive storm on 30 October 2003 and low impulsive storms on 20 November 2003 and 29 October 2003.

stochastic process, Love et al. (2015) reported that the most extreme  $Dst$  storm ( $Dst_{Min} \leq -850 \text{ nT}$ ) can occur  $\sim 1.13$  times per century, with 95% confidence level. The ICME-magnetosphere coupling function developed by Newell et al. (2007) is a good measure of the coupling efficiency.

Numerous scientific groups have studied the ionosphere-thermosphere storms using observations, theory, and models (e.g., Balan et al., 2010; Fuller-Rowell et al., 1994; Lin et al., 2005; Mendillo et al., 2006; Rishbeth, 1991; Prolss, 1995). Except at around the EIA trough (which extends up to  $\pm 25^\circ$  magnetic latitudes in extreme cases), generally positive ionospheric storms occur during daytime MPs due to the combined action of eastward prompt penetration electric field (PPEF), mechanical effects of storm time equatorward neutral wind (ENW), and daytime production of ionization. The mechanical effects of ENW raises the ionosphere to higher altitudes of reduced chemical loss and reduces (or stops) the downward diffusion of plasma to lower latitude of heavy chemical loss. The composition change effect of ENW, that is, decrease of  $O/N_2$  also happens due to the upwelling or expansion of the thermosphere almost simultaneously at mid latitudes. However, it happening at lower altitudes below about 300 km remains almost ineffective because the ionosphere has already been raised to higher altitudes by the mechanical effect of ENW. The upwelling happening at higher latitudes is balanced by downwelling causing  $O/N_2$  increase at lower latitudes (below about  $\pm 20^\circ$  magnetic latitudes) for mass conservation, as modeled by Roble et al. (1982). However, the increase of  $O/N_2$  may not be much effective in producing the positive ionospheric storms because it happens at latitudes below about  $\pm 20^\circ$  where the main process is the super plasma fountain resulting in wide and deep EIA trough (Balan et al., 2009).

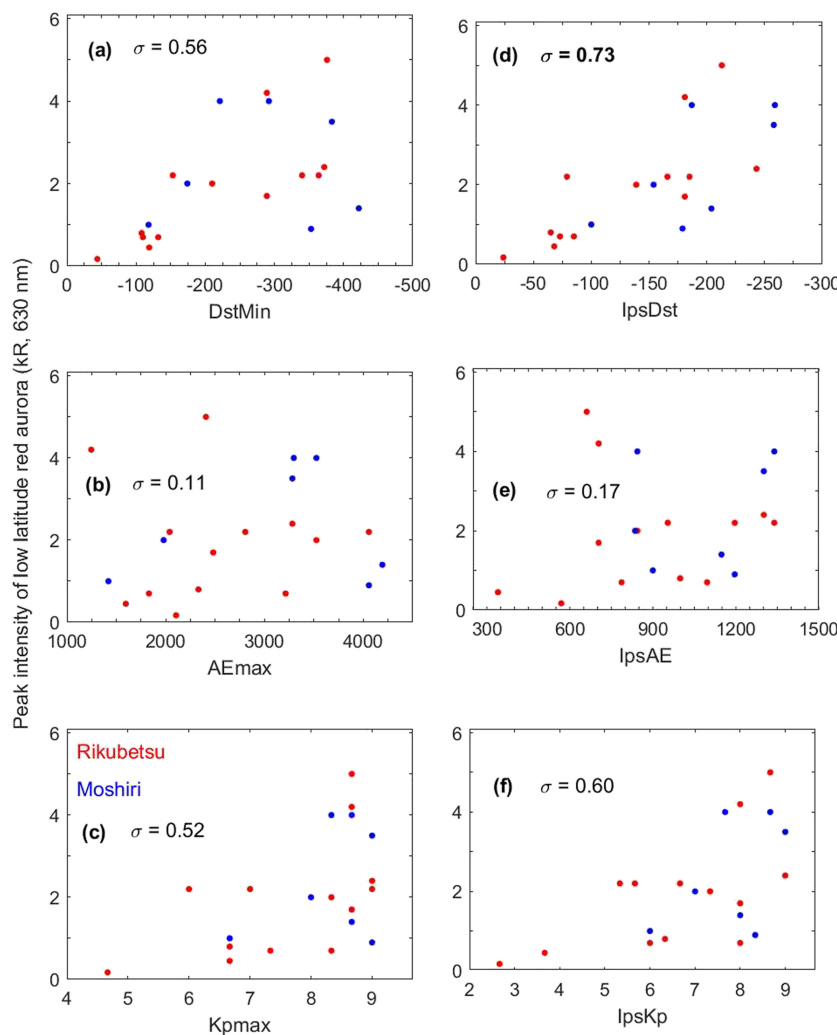


**Figure 7.** Statistics of 20 low latitude auroras, and correlations with DstMin, AE<sub>max</sub> and Kp<sub>max</sub> (a–c) and IpsDst, IpsAE, and IpsKp (d–e).

fountain (Balan et al., 2009), while positive storms occur during nighttime MPs (e.g., Sreeja et al., 2009). The latter is mainly due to the accumulation of the plasma flowing toward the equator (mechanical effects of ENW; Balan et al., 2013) with minor contributions from the composition change effect of ENW (or increase of O/N<sub>2</sub>) and reverse plasma fountain due to westward electric field (Huang et al., 2010).

Majority of the low-latitude auroras at 630 nm used in the present investigations are probably associated with stable auroral red (SAR) arcs. The auroras lasted for several hours during the MP (and early RP) of geomagnetic storms (Shiokawa et al., 2005). Considering the connection between the altitude ranges of red auroras (200–300 km) and SAR arcs (600 km), Shiokawa et al. (2005) estimates that the low-latitude auroras observed at Rikubetsu were located at latitudes higher than ~40–50° magnetic latitudes.

#### 4.1. Discussion of Present Results

The present paper has shown that the derived parameters IpsDst, IpsKp, and IpsAE representing the impulsive strength of geomagnetic storms, especially IpsDst, are better than the conventional parameters (DstMin, (dDst/dt)<sub>MPmax</sub>, Kp<sub>max</sub>, and AE<sub>max</sub>) representing the intensity of geomagnetic storms for investigating a variety of space weather aspects. The impulsive parameters (IpsDst, IpsKp, and IpsAE) giving the mean values of Dst, Kp, and AE during the MP of Dst storms (Figure 1) seem to have more systematic dependence among themselves than among their intensities (DstMin, Kp<sub>max</sub> and AE<sub>max</sub>) (Figure 2). The strength of ionosphere-

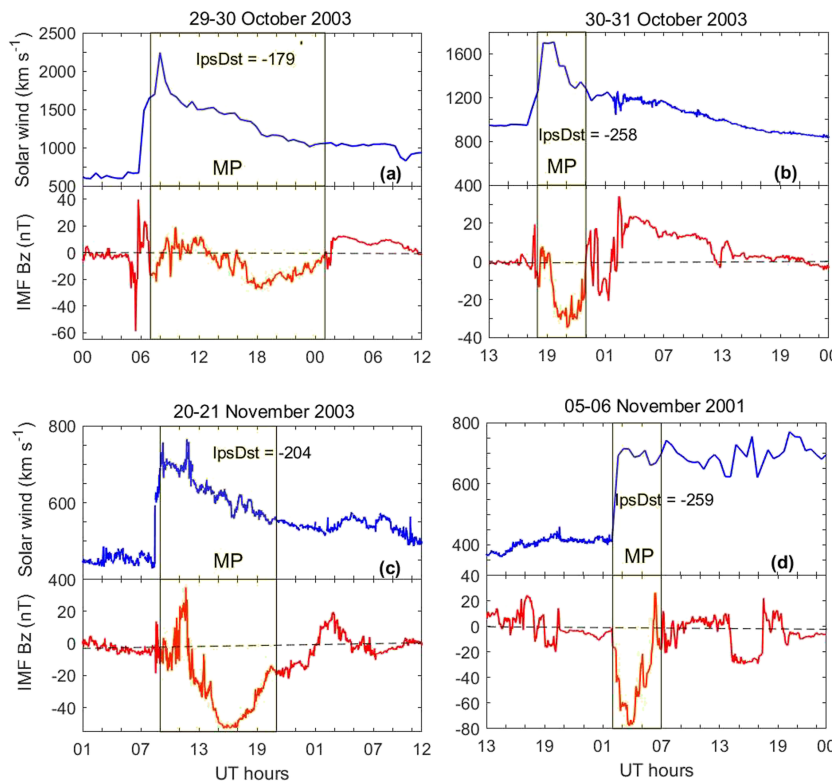


**Figure 8.** Variations of solar wind velocity  $V$  and IMF  $B_z$  corresponding to the Dst storms shown in Figure 2: (a) 29 October 2003, (b) 30 October 2003, (c) 20 November 2003, and (d) 6 November 2001.

thermosphere storms and intensity of low-latitude aurora are much stronger during high impulsive geomagnetic storms (30 October 2003 and 6 November 2003) than during high intensity geomagnetic storms as revealed by CHAMP data and optical observations (Figures 3, 4, and 6). In a statistical sense, the positive ionospheric storms ( $\triangle NmF2$ ) at midlatitudes and the intensity of low-latitude aurora correlate better with the impulsive strength of geomagnetic storms than with their intensities, and the best correlation is with  $IpsDst$  (Figures 5 and 7). It is also found that, the impulsive strength of Dst storms ( $IpsDst$ ) is a much better indicator of the ionosphere-thermosphere system responses (including auroras) than the impulsive strength of  $K_p$  and  $AE$  storms ( $IpsKp$  and  $IpsAE$ ). This seems to be due to several reasons. The  $K_p$  and  $AE$  indices do not distinguish the storm MP when majority of energy input occurs,  $K_p$  is a 3-hr index, and  $AE$  in some cases reach maximum before the main energy input begins. For these reasons,  $K_p$  and  $AE$  indices may not represent the impulsive strength of geomagnetic storms as best as the Dst index. In the case of  $AE$ , the 12 ground stations at auroral zone latitudes used to determine the index can also miss the main part of the auroral electrojet current during MP when auroral oval expands to lower latitudes.

#### 4.2. Mechanism Connecting Solar Storms

The mechanism of large  $IpsDst$  (high-energy input over short duration) probably takes place through continuous and rapid magnetic reconnection (e.g., Borovsky et al., 2008). This important physical process seems to happen when there is a simultaneous occurrence of high solar wind velocity  $V$  ( $>\sim 700 \text{ km s}^{-1}$ ) coupled with a high ICME front (or shock) velocity  $\Delta V$  (sudden increase by over  $275 \text{ km s}^{-1}$ ) and sufficiently large IMF  $B_z$  southward during the velocity increase  $\Delta V$  (Balan et al., 2014) as shown in Figure 8. The ICME event front (or shock) velocity  $\Delta V$  is the difference between the peak ICME velocity and the upstream slow solar wind velocity ( $V$ ). The velocity, especially during extreme events measured with 32-min resolution, is found to take about 2 hr to reach its peak.  $\Delta V$  in general is therefore taken as the difference between the mean

**Table 2**  
*Number, Date, IpsDst, and Solar System Parameters*

No.	Date	IpsDst (nT)	$\Delta V$ (km/s)	$\langle Bz_{\Delta V} \rangle$ (nT)	$(\Delta V \times \langle Bz_{\Delta V} \rangle)$ ( $\times 100$ km/s nT)	$\langle V_{MP} \rangle$ (km/s)	$\langle Bz_{MP} \rangle$ (nT)	$\langle V_{MP} \rangle \times \langle Bz_{MP} \rangle$ ( $\times 100$ km/s nT)
11	30 Oct 2003	-258	609	-7.67	-46.71	1458	-18.96	-276.44
2	6 Nov 2001	-259	290	-62.74	-181.95	693	-35.09	-243.17
3	29 Oct 2003	-179	1145	0.78	8.93	1,396	-3.58	-49.97
4	20 Nov 2003	-204	217	7.12	15.45	628	-25.83	-162.21

Note. The IpsDst of four super Dst storms and corresponding solar storm parameters ( $\Delta V$ ,  $\langle Bz_{\Delta V} \rangle$ ,  $(\Delta V \times \langle Bz_{\Delta V} \rangle)$ ,  $\langle V_{MP} \rangle$ ,  $\langle Bz_{MP} \rangle$ , and  $(\langle V_{MP} \rangle \times \langle Bz_{MP} \rangle)$ ).

velocity for 2 hr after and 2 hr before the start of the velocity increase. Bz at  $\Delta V(\langle Bz_{\Delta V} \rangle)$  is the mean of Bz for the two hours from the start of the velocity increase.

Figure 8 displays the variations of the velocity  $V$  and IMF Bz corresponding to the typical Dst storms and ionospheric storms (Figures 2 and 3). The important parameters  $\Delta V$ ,  $\langle Bz_{\Delta V} \rangle$ ,  $(\Delta V \times \langle Bz_{\Delta V} \rangle)$ ,  $\langle V_{MP} \rangle$ ,  $\langle Bz_{MP} \rangle$ , and  $(\langle V_{MP} \rangle \times \langle Bz_{MP} \rangle)$  are listed in Table 2. The solar storms on 30 October 2003 and 6 November 2001 have both high  $\langle V_{MP} \rangle$  and large  $\langle Bz_{MP} \rangle$  southward, as well as high  $\Delta V$  and  $\langle Bz_{\Delta V} \rangle$  southward. Their combined action leads to large IpsDst.  $\langle Bz_{MP} \rangle$  southward opens the dayside magnetopause, and high  $\Delta V$  (and high  $\langle V_{MP} \rangle$ ) provides the force for the impulsive entry of a large number of high-energy charged particles into the magnetosphere and ring current. For the solar storms on 29 October 2003 and 20 November 2003, the product  $\langle V_{MP} \rangle \times \langle Bz_{MP} \rangle$  is comparatively small. Their striking difference compared to the high impulsive events is Bz northward at the time of  $\Delta V$ , so that their impulsive action becomes ineffective. The coincidence of high  $\langle V_{MP} \rangle$  with high  $\Delta V$  and simultaneous large  $\langle Bz_{MP} \rangle$  southward leading to a steep decrease of Dst and large IpsDst was modeled (Balan, Ebihara, et al., 2017) using the comprehensive ring current model of Fok et al. (2001). The model also showed that a high  $\langle V_{MP} \rangle$  not associated with a large  $\Delta V$  and large  $\langle Bz_{MP} \rangle$  southward does not lead to large IpsDst, as observed (Balan et al., 2014).

The strong ionosphere-thermosphere storms and intense low-latitude auroras observed during storms of larger IpsDst are briefly explained here. The entry of a large number of high-energy charged particles into the ionosphere enhances the ionosphere-upper atmosphere interactions at high latitudes. This results in bright auroras extending to lower latitudes associated with intense Earthward injection of plasma sheet particles, and their high-altitude portion (i.e., red auroras) becoming visible from lower latitudes (e.g., Shiokawa et al., 2005; Tinsley et al., 1984). The good correlation of low-latitude auroral intensity with IpsDst (Figure 7) may be due to the most probable cause of the aurora involving ring current ions. The interaction between high-energy ring current ions and low-energy plasmaspheric electrons happening at the overlapping region between the ring current and the plasmasphere seems to cause the low-latitude aurora (Kozyra et al., 1987; Shiokawa et al., 2005). Because the Dst index is a proxy of the ring current ion flux, it may have good correlation with the low-latitude aurora.

The high-latitude thermosphere seems to undergo an explosive expansion due to the large Joule heating and ion-neutral frictional heating during the entry of the large number of high-energy charged particles. The explosive expansion causes the observed fast equatorward neutral surge and winds (Figure 4b). During such solar storms resulting in large IpsDst, the eastward PPEF (e.g., Kikuchi et al., 1996; Nishida, 1968; Rastogi, 1977) becomes strong as observed both on 6 November 2001 (e.g., Kikuchi et al., 2008) and 30 October 2003 (Abdu et al., 2008). The combined action of the simultaneous strong eastward PPEF and fast ENW resulted in the strong positive ionospheric storms (see also Balan et al., 2011; Mannucci et al., 2005). The observations reveal that the fast solar storms (ICMEs) with IMF Bz southward at its front leading to impulsive solar wind-magnetosphere-ionosphere-thermosphere coupling are not so common.

## 5. Summary

1. The paper has used the derived parameters (IpsDst, IpsKp, and IpsAE) representing the impulsive strength of geomagnetic storms for investigating ionosphere-thermosphere storms and low-latitude red (630 nm) aurora.

2. The impulsive parameters (IpsDst, IpsKp, and IpsAE) giving the mean values of Dst, Kp, and AE during the MP of Dst storms seem to have more systematic dependence among themselves than among their intensities (DstMin, Kp<sub>max</sub> and AE<sub>max</sub>).
3. The strength of ionosphere-thermosphere storms and intensity of low-latitude aurora are much more intense during high impulsive geomagnetic storms than during high intensity storms as revealed by CHAMP electron density (Ne) and thermospheric mass density ( $\rho$ ) data and optical observations of low-latitude red (630 nm) auroras.
4. In a statistical sense, over 175 positive ionospheric storms ( $\Delta$ NmF2) observed in 1985–2005 and the intensity of 20 red auroras observed in 1989–2004 at midlatitudes correlate better with the impulsive strength of geomagnetic storms than with their intensities, with the best correlations being with IpsDst. In short, IpsDst seems a much better parameter than other parameters for a variety of space weather applications.
5. The physical mechanism of large IpsDst (high energy input over a short duration) is investigated using the solar wind velocity  $V$  and IMF Bz measured by the ACE satellite. It involves the coincidence of high  $\langle V_{MP} \rangle$  containing a high ICME front velocity  $\Delta V$  (sudden increase by over 275 km s<sup>-1</sup>) and large  $\langle Bz_{MP} \rangle$  southward covering  $\Delta V$ . Their combined impulsive action can cause impulsive entry of a large amount of high-energy charged particles into the magnetosphere and ring current through continuous and rapid magnetic reconnection leading to large IpsDst and strong ionosphere-thermosphere response including auroras.

## Acknowledgments

We thank Hermann Lühr for the CHAMP data and scientific discussions. We acknowledge the use of Kyoto Dst <http://wdc.kugi.kyoto-u.ac.jp/dstdir/>, Kp <http://wdc.kugi.kyoto-u.ac.jp/kp/index.html>, and AE <http://wdc.kugi.kyoto-u.ac.jp/aedir/> data, CHAMP <https://isdc.gfz-potsdam.de/champ-isdc/> data, ionosonde <http://wdc.nict.go.jp/IONO/HP2009/ISDJ/index-E.html> data, and ACE satellite <http://www.srl.caltech.edu/ACE/ASC/> data. The red aurora observations are available in Shiokawa et al. (2005) and at the Institute for Space-Earth Environmental Research (ISEE), Nagoya University, Japan. This research was supported by the National Key R&D Program of China (2018YFC1407303, 2018YFC1407304), the National Natural Science Foundation of China (grants 41604139, 41574138, 41774166, 41431072, 41831072), the Chinese Meridian Project, the foundation of National Key Laboratory of Electromagnetic Environment (grants 6142403180103, 6142403180102), and JSPS KAKENHI (15H05815 and 16H06286) in Japan. Work at Los Alamos was performed under the auspices of the U.S. Department of Energy with support from the NASA-ACE program.

## References

- Abdu, M. A., de Paula, E. R., Batista, I. S., Reinisch, B. W., Matsuoka, M. T., Camargo, P. O., et al. (2008). Abnormal evening vertical plasma drift and effects on ESF and EIA over Brazil-South Atlantic sector during the 30 October 2003 super storm. *Journal of Geophysical Research*, *113*, A07313. <https://doi.org/10.1029/2007JA012844>
- Balan, N., Batista, I. S., TulasiRam, S., & Rajesh, P. K. (2016). A new geomagnetic storm parameter for the severity of space weather. *Geoscience Letters*, *3*(1), 1–5. <https://doi.org/10.1186/s40562-016-0036-5>
- Balan, N., Ebihara, Y., Skoug, R., Shiokawa, K., Batista, I. S., TulasiRam, S., et al. (2017). A scheme for forecasting severe space weather. *Journal of Geophysical Research: Space Physics*, *122*, 2824–2835. <https://doi.org/10.1002/2016JA023853>
- Balan, N., Otsuka, Y., Nishioka, M., Liu, J. Y., & Bailey, G. J. (2013). Physical mechanisms of the ionospheric storms at equatorial and higher latitudes during MP and RP of geomagnetic storms. *Journal of Geophysical Research: Space Physics*, *118*, 2660–2669. <https://doi.org/10.1002/jgra.50275>
- Balan, N., & Rao, P. B. (1990). Dependence of ionospheric response on the local time of sudden commencement and intensity of geomagnetic storms. *Journal of Atmospheric and Solar-Terrestrial Physics*, *52*(4), 269–275. [https://doi.org/10.1016/0021-9169\(90\)90094-4](https://doi.org/10.1016/0021-9169(90)90094-4)
- Balan, N., Shiokawa, K., Otsuka, Y., Kikuchi, T., Vijaya Lekshmi, D., Kawamura, S., et al. (2010). A Physical mechanism of positive ionospheric storms at low and mid latitudes through observations and modeling. *Journal of Geophysical Research*, *115*, A02304. <https://doi.org/10.1029/2009JA014515>
- Balan, N., Shiokawa, K., Otsuks, Y., Watanabe, S., & Bailey, G. J. (2009). Super plasam fountain and equatorial ionization anomaly. *Journal of Geophysical Research*, *114*, A03311. <https://doi.org/10.1029/2008JA013768>
- Balan, N., Skoug, R., TulasiRam, S., Rajesh, P. K., Shiokawa, K., Otsuka, Y., et al. (2014). CME front and severe space weather. *Journal of Geophysical Research: Space Physics*, *119*, 10,041–10,058. <https://doi.org/10.1002/2014JA020151>
- Balan, N., TulasiRam, S., Kamide, Y., Batista, I. S., Souza, J. R., Shiokawa, K., et al. (2017). Automatic selection of Dst storms and their seasonal variations in two versions of Dst in 50 years. *Earth, Planets and Space*, *69*, 59. <https://doi.org/10.1186/s40623-017-0642-2>
- Balan, N., Yamamoto, M., Liu, J. Y., Otsuka, Y., Liu, H., & Lühr, H. (2011). New aspects of thermospheric and ionospheric storms revealed by CHAMP. *Journal of Geophysical Research*, *116*, A07305. <https://doi.org/10.1029/2010JA0160399>
- Batista, I. S., de Paula, E., Abdu, M. A., Trivedi, N., & Greenspan, M. (1991). Ionospheric effects of the March 13, 1989, magnetic storm at low and equatorial latitudes. *Journal of Geophysical Research*, *96*, 13943.
- Borovsky, J. E., Hesse, M., Birn, J., & Kuzentsova, M. M. (2008). What determines the reconnection rate at the dayside magnetosphere? *Journal of Geophysical Research*, *113*, A07210. <https://doi.org/10.1029/2007JA012645>
- Burlage, L., Sittler, E., Mariani, F., & Schwenn, R. (1981). Magnetic Loop Behind an Interplanetary Shock: Voyager, Helios, and IMP 8 Observations. *Journal of Geophysical Research*, *86*, 6673–6684.
- Burton, R. K., McPherron, R. L., & Russell, C. T. (1975). An empirical relationship between interplanetary conditions and Dst. *Journal of Geophysical Research*, *80*, 4204.
- Ebihara, Y., Fok, M. C., Sazykin, S., Thomsen, M. F., Hairston, M. R., Evans, D. S., et al. (2005). Ring current and the magnetosphere-ionosphere coupling during the super storm of 20 November 2003. *Journal of Geophysical Research*, *110*, A09S22. <https://doi.org/10.1029/2004JA010924>
- Fok, M.-C., Wolf, R. A., Spiro, R. W., & Moore, T. E. (2001). Comprehensive computational model of Earth's ring current. *Journal of Geophysical Research*, *106*, 8417.
- Fuller-Rowell, T. J., Codrescu, M. V., Moffett, R. J., & Quegan, S. (1994). Response of the thermosphere and ionosphere to geomagnetic storms. *Journal of Geophysical Research*, *99*, 3893.
- Gonzalez, W. D., Joselyn, J. A., Kamide, Y., Kroehl, H. W., Rostoker, G., Tsurutani, B. T., & Vasyliunas, V. M. (1994). What is a geomagnetic storm? *Journal of Geophysical Research*, *99*, 5771.
- Gopalswamy, N., Yashiro, S., Michalek, G., Xie, H., Lepping, R. P., & Howard, R. A. (2005). Solar source of the largest geomagnetic storm of cycle 23. *Geophysical Research Letters*, *32*, L12S09. <https://doi.org/10.1029/2004GL021639>

- Green, J. C., Likar, J., & Shprits, Y. (2017). Impact of space weather on the satellite industry. *Space Weather*, 15, 804–818. <https://doi.org/10.1002/2017SW001646>
- Hayakawa, H., Ebihara, Y., Hand, D. P., Hayakawa, S., Kumar, S., Mukherjee, S., & Veenadhari, B. (2018). Low-latitude aurorae during the extreme space weather events in 1859. *The Astrophysical Journal*, 869, 57.
- Huang, C. M., Chen, M. Q., & Liu, J. Y. (2010). Ionospheric positive stormphases at the magnetic equator close to sunset. *Journal of Geophysical Research*, 115, A07315. <https://doi.org/10.1029/2009JA014936>
- Kamide, Y., Baumjohann, W., Daglis, I. A., Gonzalez, W. D., Grande, M., Joselyn, J. A., et al. (1998). Current understanding of magnetic storms: Storm-substorm relationships. *Journal of Geophysical Research*, 103(A8), 17,705–17,728. <https://doi.org/10.1029/98JA01426>
- Kataoka, R., Isobe, H., Hayakawa, H., Tamazawa, H., Kawamura, A. D., Miyahara, H., et al. (2017). Historical space weather monitoring of prolonged aurora activities in Japan and in China. *Space Weather*, 15, 392–402. <https://doi.org/10.1002/2016SW001493>
- Kikuchi, T., Hashimoto, K. K., & Nozaki, K. (2008). Penetration of magnetospheric electric fields to the equator during a geomagnetic storm. *Journal of Geophysical Research*, 113, A06214. <https://doi.org/10.1029/2007JA012628>
- Kikuchi, T., Luhr, H., Kitamura, T., Saka, O., & Schlegel, K. (1996). Direct penetration of the polar electric fields to the equator during a DP 2 event as detected by the auroral and equatorial magnetometer chains and the EISCAT radar. *Journal of Geophysical Research*, 101, 17,161–17,173.
- Klimas, A. J., Vassiliadis, D., & Baker, D. N. (1997). Data-derived analogues of the magnetospheric dynamics. *Journal of Geophysical Research*, 102, 26,993.
- Kozyra, J. U., Shelley, E. G., Comfort, R. H., Brace, L. H., Cravens, T. E., & Nagy, A. F. (1987). The role of ring current O<sup>+</sup> in the formation of stable auroral red arcs. *Journal of Geophysical Research*, 92, 7487–7502.
- Liemohn, M. W., Jaszowski, M., Kozyra, J. U., Ganushkina, N., Thomsen, M. F., & Borovsky, J. E. (2010). CIR versus CME drivers of the ring current during intense magnetic storms. *Proceedings of the Royal Society A*, 466, 3305–3328. <https://doi.org/10.1098/rspa.2010.0075>
- Lin, C. H., Richmond, A. D., Heelis, R. A., Bailey, G. J., Lu, G., Liu, J. Y., et al. (2005). Theoretical study of the low- and mid latitude ionospheric electron density enhancement during the October 2003 super storm: Relative importance of the neutral wind and the electric field. *Journal of Geophysical Research*, 110, A12312. <https://doi.org/10.1029/2005JA011304>
- Liu, H., & Luhr, H. (2005). Strong disturbance of the thermospheric density due to storms: CHAMP observations. *Journal of Geophysical Research*, 110, A09S29. <https://doi.org/10.1029/2004JA010908>
- Loomis, E. (1861). On the great auroral exhibition of Aug. 28th to Sept. 4th, 1859, and on auroras generally—8th article. *American Journal of Science*, 32, 318–335.
- Love, J. J., & Gannon, J. L. (2009). Revised Dst and the epicycles of magnetic disturbance: 1958–2007. *Annales de Geophysique*, 28(8), 3101–3131. <https://doi.org/10.5194/angeo-27-3101>
- Love, J. J., Rigler, E. J., Pulkkinen, A., & Riley, P. (2015). On the lognormality of historical magnetic storm intensity statistics: Implications for extreme-event probabilities. *Geophysical Research Letters*, 42, 6544–6553. <https://doi.org/10.1002/2015GL064842>
- Lu, G., Goncharenko, L. P., Nicolls, M. J., Maute, A. I., Coster, A. J., & Paxton, L. J. (2012). Ionospheric and thermospheric variations associated with prompt penetration electric fields. *Journal of Geophysical Research*, 117, A08312. <https://doi.org/10.1029/2012JA017769>
- Lühr, H., Xiong, C., Olsen, N., & Le, G. (2017). Near-Earth magnetic field effects of large-scale magnetospheric currents. *Space Science Reviews*, 206(1–4), 521–545. <https://doi.org/10.1007/s11214-016-0267-y>
- Mannucci, A. J., Tsurutani, B. T., Iijima, B. A., Komjathy, A., Saito, A., Gonzalez, W. D., et al. (2005). Dayside global ionospheric response to the major interplanetary events of October 29–30, 2003 Halloween Storms. *Geophysical Research Letters*, 32, L12S02. <https://doi.org/10.1029/2004GL021467>
- Mayr, H. G., & Volland, H. (1973). Magnetic storm characteristics of the thermosphere. *Journal of Geophysical Research*, 78, 2251.
- McComas, D. J., Bame, S. J., Barker, P., Feldman, W. C., Phillips, J. L., & Riley, P. (1998). Solar wind electron proton alpha monitor (SWEPAM) for the advanced composition explorer. *Space Science Reviews*, 86, 563–612.
- Mendillo, M. (2006). Storms in the ionosphere: Patterns and processes for total electron content. *Reviews of Geophysics*, 44, RG4001. <https://doi.org/10.1029/2005RG000193>
- Newell, P. T., Sotirelis, T., Liou, K., Meng, C.-I., & Rich, F. J. (2007). A nearly universal solar wind-magnetosphere coupling function inferred from 10 magnetospheric state variables. *Journal of Geophysical Research*, 112, A01206. <https://doi.org/10.1029/2006JA012015>
- Nishida, A. (1968). Coherence of geomagnetic DP2 magnetic fluctuations with interplanetary magnetic variations. *Journal of Geophysical Research*, 73(17), 5549–5559.
- Prolss, G. W. (1995). Ionospheric F region storms. In H. Volland (Ed.), *Handbook of atmospheric electrodynamics* (pp. 195–248). Boca Raton: CRC Press.
- Rassoul, H. K., Rohrbaugh, R. P., & Tinsley, B. A. (1992). Low-latitude particle precipitation and associated local magnetic disturbances. *Journal of Geophysical Research*, 97, 4041–4052.
- Rastogi, R. G. (1977). Geomagnetic storms and electricfields in the equato-rial ionosphere. *Nature*, 268, 422.
- Reigber, C., Luhr, H., & Schwintzer, P. (2002). CHAMP mission status. *Advances in Space Research*, 30, 129–134.
- Rishbeth, H. (1991). F-region storms and thermospheric dynamics. *Journal of Geomagnetism and Geoelectricity*, 43, 513.
- Roble, R. G., Dickinson, R. E., & Ridley, E. C. (1982). Global circulation and temperature structures of thermosphere with high-latitude convection. *Journal of Geophysical Research*, 87, 1599.
- Rostoker, G., Samson, J. C., Creutzberg, F., Hughes, T. J., McDiarmid, D. R., McNamara, A. G., et al. (1995). CANOPUS: A ground based instrument array for remote sensing the high latitude ionosphere during the ISTP/GGS program. *Space Science Reviews*, 46, 743.
- Shiokawa, K., Katoh, Y., Satoh, M., Ejiri, M. K., Ogawa, T., Nakamura, T., et al. (1999). Development of optical mesosphere thermosphere imagers (OMTI). *Earth, Planets and Space*, 51, 887–896.
- Shiokawa, K., Miyoshi, Y., Brandt, P. C., Evans, D. S., Frey, H. U., Goldstein, J., & Yumoto, K. (2013). Ground and satellite observations of low-latitude red auroras at the initial phase of magnetic storms. *Journal of Geophysical Research: Space Physics*, 118, 256–270. <https://doi.org/10.1029/2012JA018001>
- Shiokawa, K., Ogawa, T., & Kamide, Y. (2005). Low-latitude auroras observed in Japan: 1999–2004. *Journal of Geophysical Research*, 110, A05202. <https://doi.org/10.1029/2004JA010706>
- Singh, A. K., Singh, D., & Singh, R. P. (2010). Space Weather: Physics, Effects and Predictability. *Surveys in Geophysics*, 31, 581–638. <https://doi.org/10.1007/s10712-010-9103-1>
- Skoug, R. M., Gosling, J. T., Steinberg, J. T., McComas, D. J., Smith, C. W., Ness, N. F., et al. (2004). Extremely high speed solar wind: 29–30 October 2003. *Journal of Geophysical Research*, 109, A09102. <https://doi.org/10.1029/2004JA010494>
- Sojka, J. J., Davis, M., Schunk, R. W., & Heelis, R. A. (2012). A modellingstudy of the longitudinal dependence of storm time midlatitude dayside total electron content enhancements. *Journal of Geophysical Research*, 117, A02315. <https://doi.org/10.1029/2011JA017000>

- Sreeja, V., Ravindran, S., Pant, T. K., Devasia, C. V., & Paxton, L. J. (2009). Equatorial and low latitude ionosphere thermosphere system response to the space weather event of August 2005. *Journal of Geophysical Research*, *114*, A12307. <https://doi.org/10.1029/2009JA014491>
- Sugiura, M. (1964). Hourly values of equatorial Dst for the IGY. In *Ann. Int. Geophysical Year* (Vol. 35, pp. 9–45). New York: Pergamon.
- Sugiura, M., & Kamei, T. (1991). Equatorial Dst index 1957–1957–1986. In A. Berthelier, & M. Menville (Eds.), *LAGA bull 40*, Saint-Maur-des-Fosses: International Service of Geomagnetic Indices.
- Svalgaard, L. (1977). Geomagnetic activity: Dependence on solar wind parameters. In J. B. Zirker (Ed.), *Coronal Holes and High Speed Wind Streams* (pp. 371–441). Boulder: Colo. Assoc. Univ. Press.
- Tinsley, B. A., Rohrbaugh, R. P., Rassoul, H., Barker, E. S., Cochran, A. L., Cochran, W. D., et al. (1984). Spectral characteristics of two types of low latitude aurorae. *Geophysical Research Letters*, *11*, 572–575.
- Tulasi Ram, S., Balan, N., Veenadhari, B., Gurubaran, S., Ravindran, S., Tsugawa, T., et al. (2012). First observational evidence for opposite zonal electric fields in equatorial E and F region altitudes during a geomagnetic storm period. *Journal of Geophysical Research*, *117*, A09318. <https://doi.org/10.1029/2012JA018045>
- Tulasi Ram, S., Yokoyama, T., Otsuka, Y., Shiokawa, K., Sripathi, S., Veenadhari, B., et al. (2015). Duskside enhancement of equatorial zonal electric field response to convection electric fields during the St. Patrick's Day storm on 17 March 2015. *Journal of Geophysical Research: Space Physics*, *121*, 538–548. <https://doi.org/10.1002/2015JA021932>
- Vijaya Lekshmi, D., Balan, N., Tulasi Ram, S., & Liu, J. Y. (2011). Statistics of geomagnetic storms and ionospheric storms at low and mid latitudes in two solar cycles. *Journal of Geophysical Research*, *116*, A11328. <https://doi.org/10.1029/2011JA017042>
- Witasse, O., Sánchez-Cano, B., Mays, M. L., Kajdič, P., Opgenoorth, H., Elliott, H. A., et al. (2017). Interplanetary coronal mass ejection observed at STEREO-A, Mars, comet67P/Churyumov-Gerasimenko, Saturn, and New Horizons route to Pluto: Comparison of its Forbush decreases at 1.4, 3.1, and 9.9 AU. *Journal of Geophysical Research: Space Physics*, *122*, 7865–7890. <https://doi.org/10.1002/2017JA023884>
- Zhu, D., Billings, S. A., Balikhin, M. A., Wing, S., & Alleyne, H. (2007). Multi-input data derived Dst model. *Journal of Geophysical Research*, *112*, A06205. <https://doi.org/10.1029/2006JA012079>